JOURNAL
OF
THE ROYAL
SOCIETY

Interface

Hemispherical Brillouin zone imaging of a diamond-type biological photonic crystal

Bodo D. Wilts, Kristel Michielsen, Hans De Raedt and Doekele G. Stavenga

Supplementary data	"Data Supplement" http://rsif.royalsocietypublishing.org/content/suppl/2011/12/14/rsif.2011.0730.DC1.html
References	**This article cites 31 articles, 8 of which can be accessed free** http://rsif.royalsocietypublishing.org/content/early/2011/12/14/rsif.2011.0730.full.html#ref-list-1 **Article cited in:** http://rsif.royalsocietypublishing.org/content/early/2011/12/14/rsif.2011.0730.full.html#related-urls
P<P	Published online 21 December 2011 in advance of the print journal.
Email alerting service	Receive free email alerts when new articles cite this article - sign up in the box at the top right-hand corner of the article or click **here**

Advance online articles have been peer reviewed and accepted for publication but have not yet appeared in the paper journal (edited, typeset versions may be posted when available prior to final publication). Advance online articles are citable and establish publication priority; they are indexed by PubMed from initial publication. Citations to Advance online articles must include the digital object identifier (DOIs) and date of initial publication.

To subscribe to *J. R. Soc. Interface* go to: **http://rsif.royalsocietypublishing.org/subscriptions**

Hemispherical Brillouin zone imaging of a diamond-type biological photonic crystal

**Bodo D. Wilts[1],*, Kristel Michielsen[2], Hans De Raedt[1]
and Doekele G. Stavenga[1]**

[1]*Computational Physics, Zernike Institute for Advanced Materials, University of Groningen, Nijenborgh 4, 9747 AG, Groningen, The Netherlands*
[2]*Institute for Advanced Simulation, Jülich Supercomputing Centre, Research Centre Jülich, 52425 Jülich, Germany*

The brilliant structural body colours of many animals are created by three-dimensional biological photonic crystals that act as wavelength-specific reflectors. Here, we report a study on the vividly coloured scales of the diamond weevil, *Entimus imperialis*. Electron microscopy identified the chitin and air assemblies inside the scales as domains of a single-network diamond ($Fd3m$) photonic crystal. We visualized the topology of the first Brillouin zone (FBZ) by imaging scatterometry, and we reconstructed the complete photonic band structure diagram (PBSD) of the chitinous photonic crystal from reflectance spectra. Comparison with calculated PBSDs indeed showed a perfect overlap. The unique method of non-invasive hemispherical imaging of the FBZ provides key insights for the investigation of photonic crystals in the visible wavelength range. The characterized extremely large biophotonic nanostructures of *E. imperialis* are structurally optimized for high reflectance and may thus be well suited for use as a template for producing novel photonic devices, e.g. through biomimicry or direct infiltration from dielectric material.

Keywords: photonic bandgap materials; structural colour; Coleoptera; biomimetics; biomaterials; iridescence

1. INTRODUCTION

The brilliant, iridescent body colours of many beetles, birds, butterflies and fish are created by the interaction of light with nanostructured materials in the animals' outer body layers, i.e. their exoskeleton, feathers and scales [1–4]. Beetles and weevils, in particular, employ a large range of photonic structures to produce iridescence, e.g. multi-layers [5], birefringent or dichroic circular polarizing layers [6] and three-dimensional biological photonic crystals [7,8]. The refractive index of these structures is periodically modulated on the length scale of visible light, so that (constructive) interference of light is observed in this wavelength range [2,4,9]. Photonic crystals are thus the optical analogue of semiconductor crystals in that the photonic structure creates photonic bandgaps, over which a range of wavelengths of light can be neither emitted nor propagated [9].

In insects, three-dimensional photonic crystals are usually fabricated by interconnecting networks of air (refractive index, $n = 1$) and the dielectric cuticular biomaterial chitin ($n = 1.56$) [10,11] that form usually one of the three simplest triply periodic bicontinuous cubic minimal surfaces: primitive cubic (P), diamond (D) or gyroid (G) [12–15]. A precise characterization of photonic crystals reflecting in the visible wavelength range is critical to understand their optical and biological function. Structural knowledge of the biological photonic crystals will further inspire the design and replication of biomimetic devices [16,17]. Presently, the routine production of artificial, visibly active photonic crystals is still a considerable challenge [18–20].

A precise angular-resolved measurement of the photonic band structure diagram (PBSD) of three-dimensional biological photonic crystals is still lacking, as previous publications have mainly focused on partial photonic bandgaps in high-symmetry directions [7,14,21]. Here, we apply hemispherical Brillouin zone imaging using imaging scatterometry [22] to completely characterize the three-dimensional biological photonic crystal structures in the wing scales of the diamond weevil, *Entimus imperialis*. We measured the complete PBSD and determined the symmetry of the underlying unit cell structure of the photonic crystal by imaging the topology of the first Brillouin zone (FBZ), a unique identifier of the structural symmetry.

2. MATERIAL AND METHODS

2.1. Animals

A specimen of the diamond weevil, *E. imperialis* (Forster 1771; Curculionidae: Entiminae: Entimini), of the

*Author for correspondence (b.d.wilts@rug.nl).

Electronic supplementary material is available at http://dx.doi.org/10.1098/rsif.2011.0730 or via http://rsif.royalsocietypublishing.org.
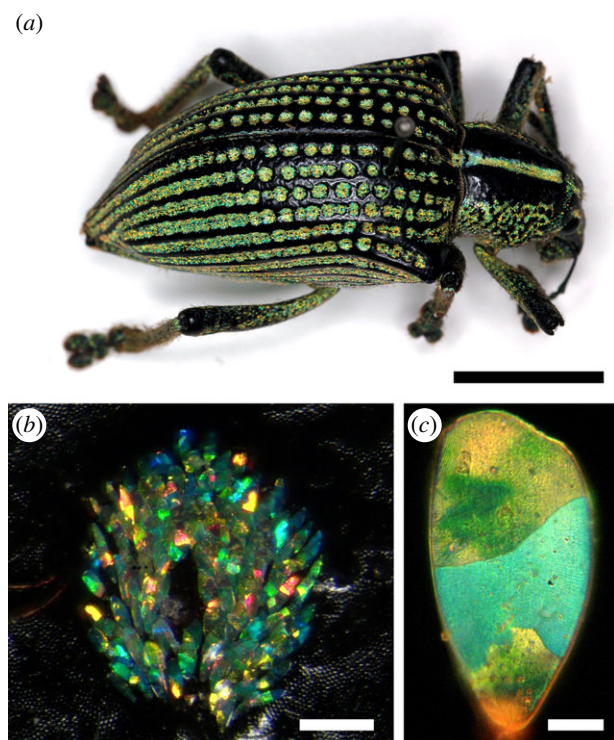
Figure 1. The diamond weevil, *Entimus imperialis*, and its scale organization. (*a*) The intact animal with the black elytra where numerous pits are studded with yellow-green scales. Scale bar, 1 cm. (*b*) A single pit as seen in an epi-illumination microscope, showing highly reflective scales of different colours. Scale bar, 200 μm. (*c*) A single scale with a few differently coloured domains. Scale bar, 20 μm.

Figure 2. Microstructure of the scales of *Entimus imperialis*. (*a*) Highly magnified image of a single scale at a zone boundary. Note the different lamellar arrangements in the two areas. Scale bar, 5 μm. (*b*) Scanning electron microscopy of a cross section of a fractured scale showing a highly organized interior of tilted sheets with square symmetry. Scale bar, 2 μm. (*c*) Transmission electron microscopy (TEM) image of the nanostructure of an *E. imperialis* scale. The red-bordered inset shows a simulated $(3\,2\,12)$ TEM cross section of a level-set single-network diamond-type crystal. Scale bar, 2 μm.

Coleoptera collection in the Natural History Museum Naturalis (Leiden, The Netherlands; curator Dr J. Krikken) was photographed by a Canon EOS 30D camera equipped with an F70 macro-objective and a Nikon SB-800 flash (figure 1*a*). Details of the scale arrangement on the elytra of a specimen obtained from Prof. J.-P. Vigneron (University of Namur, Belgium) were photographed by a Zeiss Universal Microscope (Carl Zeiss AG, Oberkochen, Germany), applying epi-illumination and using a Kappa DX-40 digital camera (Kappa Optronics GmbH, Gleichen, Germany; figures 1*b,c* and 2*a*).

2.2. Electron microscopy

The structure of the wing scales was investigated, after sputtering with palladium, by scanning electron microscopy (SEM) using a Philips XL-30 ESEM (Philips, Eindhoven, The Netherlands) and by transmission electron microscopy (TEM) using a Philips CM-100 bioelectron microscope operated at 80 kV. For TEM, the scales were embedded in a mixture of Epon and Araldite, following a standard embedding procedure [5].

2.3. Imaging scatterometry

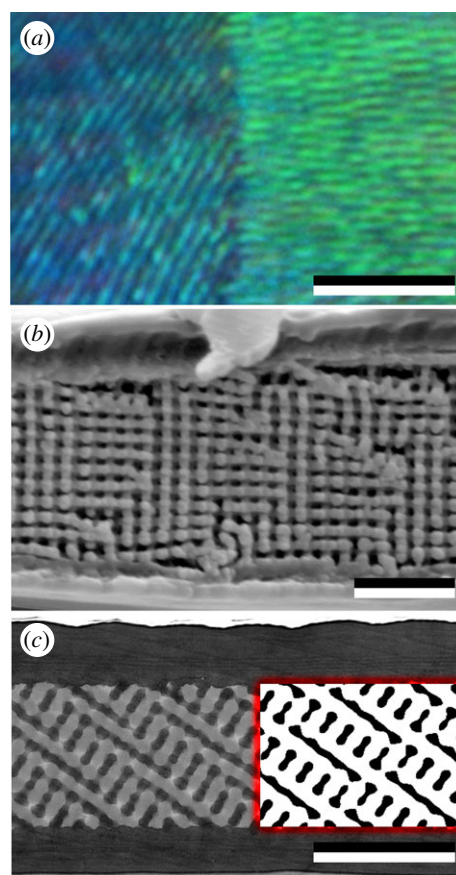The far-field angular distribution of the light scattered from single domains on single scales (figure 3), glued to the end of pulled glass micropipettes, was visualized by an imaging scatterometer [22]. The scatterometer is built around an ellipsoidal mirror that collects light from a full hemisphere around its first focal point where the sample is positioned. A xenon lamp was used for illumination and the spot size diameter was approximately 15 μm. A small piece of magnesium oxide served as a white diffuser reference object. Scatterogram images were acquired by an Olympus DP70 camera and were subsequently corrected for geometrical distortions using a Matlab routine. Reflectance spectra (figure 4*a,b*) were measured by a CCD detector array spectrometer (AvaSpec-2048-2; Avantes, Eerbeek, The Netherlands) with an effective aperture of approximately 4° [5].

2.4. Photonic band structure diagram simulations

PBSDs for the single-network diamond photonic crystal in a face-centred cubic (FCC) basis were simulated by the MIT photonics bandgap package (http://ab-initio.mit.edu/mpb) [23]. The dielectric function was
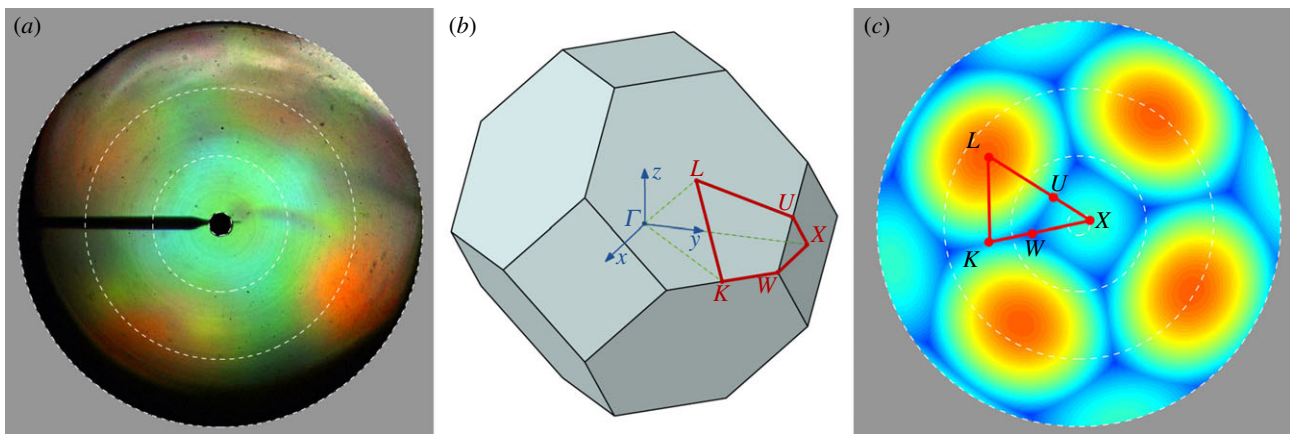
Figure 3. Hemispherical imaging of the first Brillouin zone (FBZ) of a single-network diamond photonic crystal. (*a*) Image of the hemispherical reflectance of a single-scale domain. The shadow of the glass pipette holding the scale is seen at 09.00. The white-dashed circles indicate scattering angles of 5°, 30°, 60° and 90°. (*b*) Sketch of the FBZ of a diamond-type crystal showing high-symmetry points (L–U–X–W–K) forming the irreducible BZ (red line). The (*1 0 0*) orientation is pointing upwards. (*c*) Simulated scatterogram of an ideal diamond-type photonic crystal, approximating a (*7 7 1*) orientation. The spatial directions corresponding to the irreducible BZ and the high-symmetry points are indicated.

generated using the level-set equation for a single diamond structure by [12,13,24]:

$$\cos z \sin(x+y) + \sin z \cos(x-y) = t, \qquad (2.1)$$

where the parameter t determines the filling fraction of each network in the unit cell. To simulate a dielectric single-network diamond structure, the dielectric function $f(x,y,z)$ was chosen such that $n(x,y,z) = 1.56$ if $f(x,y,z) \leq t$, and $n(x,y,z) = 1$ if $f(x,y,z) > t$, where $n(x,y,z)$ is the refractive index at the point (x,y,z) of the unit cell. We confirmed our photonic band structure model by changing the dielectric constant of the material to that of silicon ($\epsilon = 11.9$) to match the calculations of Michielsen & Kole [24]. As an additional check, we changed the topology to a chitin-based single-network gyroid and found full agreement with the results of Saranathan *et al.* [14].

3. RESULTS AND DISCUSSION

The diamond weevil, *E. imperialis*, a large weevil mainly found in Brazil [25], appeared to be ideal for studying the photonic responses of biological photonic crystals. The weevil's body is marked by rows of bright green dots on an otherwise black body (figure 1*a*). Investigation of the elytra by a light microscope reveals that the shiny dots are pits decorated with numerous scales, each of which has large, coloured domains with highly directional reflections (figure 1*b*). Upon slight rotation of the scales, reflecting domains vanish and new ones appear. These amazing scales have been studied since the early twentieth century [2]. *Entimus imperialis* appears to be unique when compared with related weevils [7,26,27], but also butterflies [13,14], in that its scales have very large photonic domains, up to approximately 50 μm^2 in size (figure 1*c*), a factor of 5–10 larger in size than the photonic domains found in other species. The colours of the domains range from cyan blue to yellow orange.

In the differently coloured domains, distinctly oriented lines can be observed (figure 2*a*), suggesting the presence of an ordered photonic structure inside the scales. Therefore, we examined the internal scale structure by SEM and TEM. In SEM, the interior of the scales appeared to contain highly ordered stacks of chitinous sheets with air cavities, having either square or hexagonal symmetry, enveloped by a thin film cortex of roughly 1 μm thickness (figure 2*b* and electronic supplementary material, figure S1). To fully characterize the structure, we matched TEM cross sections with cross sections derived from various level-set minimal surface models (figure 2*c*, inset) [12–14,28]. The observed motifs are characteristic for simulated cross sections of single-network diamond crystals (point group $Fd3m$). No overlap with single-network gyroid ($I4_1 32$) or simple primitive ($Pm3m$) cross sections was observed. We thus concluded that the chitinous structure inside the scales is a single-network diamond photonic crystal. The photonic crystals inside the scales form a layer of fused photonic crystal domains, similar to the wing scales of certain papilionid butterflies with single-network gyroid photonic crystals [4,14].

The material composition, and thus the material filling fraction, of a single-network diamond photonic crystal can be expressed by the level-set parameter t that defines the triply periodic intermaterial dividing surface (IMDS). In real space, the network is defined by the Schwartz D minimal surface via equation (2.1). Quantitative analysis of different regions in individual scales as well as matching of TEM cross sections with the computationally simulated level-set cross sections yielded a cubic lattice constant $a = 445 \pm 10$ nm and a level-set parameter $t = -0.50 \pm 0.08$, corresponding to a chitin filling fraction of 0.30 ± 0.04. The obtained values are comparable with the anatomical characteristics reported for scales of other beetles with a chitinous diamond photonic crystal [7,8]. The cubic lattice constant parameters for butterflies with gyroid-type photonic crystals are considerably smaller, while the chitin filling fraction is comparable [13,28].

We have used the scales of the diamond weevil to directly visualize various symmetry orientations and the angular spectral response of differently oriented
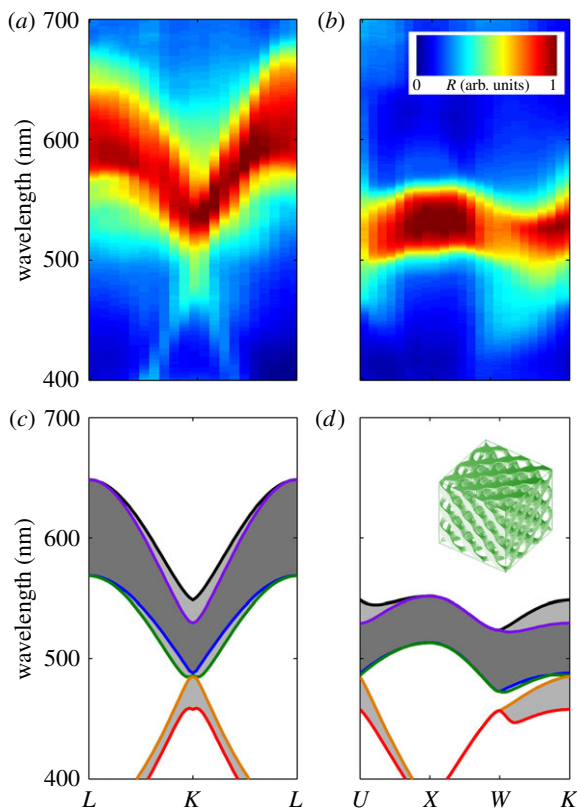
Figure 4. Photonic band structure diagrams (PBSDs). Measured (a,b) and simulated (c,d) PBSDs for a single-network diamond-type photonic crystal $(Fd3m)$ along the paths (a,c) $L–K–L$ and (b,d) $U–X–W–K$, respectively. The grey areas in (c,d) indicate the photonic bandgap of the investigated structure, corresponding to the measured reflectance bands in (a,b). In the simulation, the dielectric constant was $\epsilon = 2.45$ and the chitin filling fraction was approximately 0.3 $(t = -0.5)$. For the wavelength conversion in (c,d), the cubic lattice constant of the photonic crystal was set to $a = 445$ nm (see also electronic supplementary material, figure S4). The inset shows a rendered model of the single diamond photonic crystal.

individual photonic crystals using imaging scatterometry [22]. The point spread function for narrow beam illumination appeared to be equal to the angular width of the incoming light beam (electronic supplementary material, figure S2). This allowed illumination of single-scale domains with a wide-aperture white-light beam to obtain an aberration-free image of the complete hemispherical reflectance [5]. We found distinct orientations of (large) orange and (small) green faces, surrounded by a cyan blue-coloured border (figure 3a). The green faces are surrounded by four orange faces and thus have a fourfold symmetry, whereas the orange faces have a sixfold symmetry and are surrounded each by three orange and three green faces.

The microstructure and orientation of a photonic crystal determines the photonic response to incident light. Photonic crystals with a complete photonic bandgap have an angle-independent reflection in a certain wavelength range. However, most biological photonic crystals do not possess a complete photonic bandgap, owing to the small refractive index contrast n'/n of organic material against air (for chitin and air this

contrast is $n'/n = 1.56$ [9–11]. For photonic structures with a low refractive index contrast, the orientation of the crystal becomes highly important because a change in the crystal orientation or the angle of light incidence causes a different reflectance spectrum. Generally, the faces of the FBZ fulfil Bragg's law and thus approximately determine the peak wavelength of the reflected light, or, more accurately, the central wavelength of the photonic bandgap [28]. The FBZ is the primitive cell of the structure in reciprocal space and thus is inevitably connected to the symmetry of the unit cell in reciprocal space [9]. A single-network diamond photonic crystal has a FCC unit cell in real space, and therefore the faces of the FBZ form a truncated octahedron having eight hexagonal and six smaller square faces with base-centred cubic symmetry (BCC; figure 3b). High-symmetry points in the FBZ are of special interest, because they form the irreducible BZ, a diagnostic characteristic for any given photonic structure [9,28].

To see whether the measured hemispherical reflectance profile is directly connected to the structure of the FBZ, we simulated the spatial reflection pattern from an ideal diamond crystal structure for different orientations. Indeed, a diamond crystal with $(7\,7\,1)$ orientation closely matches the measured reflectance profile (figure 3a,c). The symmetry and size of the coloured areas directly correspond to the different faces of the truncated octahedron forming the FBZ (figure 3; cf. Poladian *et al.* [28]). The hemispherical reflectance profile does not conform to the predictions from alternative cubic minimal surfaces as P or single G. For both of these cubic minimal surfaces, the spatial scattering is predicted to be very different in shape as well as in the spectral width (electronic supplementary material, figure S3). The observed aberrations at scattering angles greater than 70° can be attributed to the slight curvature of the investigated scales (figure 1c and electronic supplementary material, S2).

Although the FBZ for a diamond photonic crystal has been assessed in the microwave regime [29], here we for the first time measured the FBZ for a diamond photonic crystal reflecting visible light. Mapping the topology of the FBZ by imaging of the angle-dependent reflectance allows direct, non-invasive discrimination of different crystal types as well as their orientation. Previously, this was possible only via indirect TEM methods and subsequent mapping of crystal orientations [7,13,14].

The PBSD determines the reflectance and the iridescence of a given crystal structure. A spectrophotometer connected to the imaging scatterometer allowed measurement of the reflectance spectrum in angular areas of approximately 4° at any given point of the scatterogram [5]. Figure 4a,b shows band structure diagrams of the diamond weevil's diamond biological photonic crystal measured along two user-defined paths in the scatterograms. This flexible measurement is a significant improvement on previous techniques that were limited to measurements along linear rotations of goniometers [29]. Note that the reflectance spectra in essence measure the photonic bandgap diagram. The larger the photonic bandgap width in a particular direction, i.e. the distance between two adjacent photonic bands, the broader is the

expected reflectance spectrum (corresponding to different shades of grey in figure 4*c*,*d*). We calculated the PBSD of a single diamond photonic crystal by modelling the photonic crystal in the scales of *E. imperialis*, using the MIT photonic band structure package and the structural parameters obtained from electron microscopy (figure 4*c*,*d* and electronic supplementary material, figure S4) [9,23]. In the simulation, the dielectric constant of the chitin network was set to $\epsilon = n^2 \approx 2.45$ (index-matching experiments yielded a real refractive index of the chitin $n = 1.56$; scale absorption was negligible). We found excellent agreement between the measured and simulated PBSDs (figure 4). Therefore, by measuring the angular spectral dependency in addition to the topology of the FBZ, we can completely characterize the structure of any photonic crystal.

The spectral measurements provide additional insight, as they are characteristic for the investigated crystal type. For instance, the maximal wavelength ratio in the spectral state space, i.e. the range of observable spectra reflected from the structure, depends on the type of crystal. For diamond-, gyroid- and simple cubic-type photonic crystals the maximal peak wavelength ratio is 1.29, 1.41 and 1.72, respectively [28]. For *E. imperialis*, we determined a ratio of 1.27 ± 0.05, confirming the theoretical prediction for a single diamond photonic crystal.

Interestingly, the complex three-dimensional arrangement of air and chitin in the wing scales of the diamond weevil may provide an ideal template to achieve a complete photonic bandgap material that reflects in the visible wavelength range, especially because photonic crystals with the largest photonic bandgap are based on the diamond morphology [20]. We thus investigated the dependency of the photonic bandgap width, i.e. the Q-factor or gap–midgap ratio $\Delta\omega/\omega_{\mathrm{m}}$, where ω_{m} is the midgap frequency and $\Delta\omega$ is the bandgap width of the partial bandgap in the high-symmetry direction [9], for different filling fractions of the chitin network by varying the threshold parameter of the IMDS (figure 5). A relatively broad plateau of maximal reflectance results for chitin filling fractions between 0.3 and 0.4. Indeed, for the material filling fraction of 0.30 ± 0.04, the value found for the scales of *E. imperialis*, the bandgap width is close to optimal for creating a maximal photonic response, as here the partial bandgaps are largest.

We further investigated the refractive index dependency of the diamond photonic crystal and found that a complete photonic bandgap opens for relatively low refractive index contrasts of $n'/n \sim 2$ when using the filling fraction of the diamond weevil scales (electronic supplementary material, figure S5; see also Galusha *et al.* [30]). A photonic structure with this refractive index contrast can be achieved by direct dielectric infiltration [30] or metal coating [31], whereas a change of the unit cell size could be achieved by hydrogel infiltration [32]. The uncommonly large single-network diamond biological photonic crystals of *E. imperialis* will thus be a well-suited template to further explore the photonic properties of visibly active photonic crystals that could ultimately lead to novel, efficient optical devices as, for example, all-integrated optical circuits [33] or high-efficiency solar cells [34].
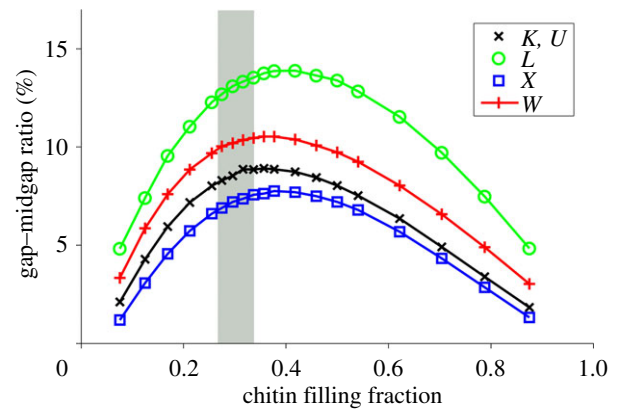

Figure 5. Filling factor dependency of the partial photonic bandgap widths for single diamond photonic crystals. Gap–midgap ratios are shown for the partial bandgaps along the high-symmetry directions $K = U$, L, W and X. The observed filling fraction for the wing scales of *Entimus imperialis* is shown in grey; the dielectric constant of the biomaterial chitin was $\epsilon = 2.45$. The filling fraction of the weevil scales is on the lower edge of the optimal reflectance plateau, indicating an optimal weight–reflectance ratio.

4. CONCLUSIONS

The presented technique of hemispherical Brillouin zone imaging using an imaging scatterometer permits the complete non-destructive assessment of important photonic parameters of any photonic bandgap material because it is not limited to biological samples. We have shown that the type and orientation of individual, differently oriented biological photonic crystals of the diamond weevil can be assessed by direct visualization of the FBZ. Furthermore, the complete PBSD of a biological photonic crystal could be measured for any given direction in the hemispherical reflectance image. Therefore, the pureness of artificially created photonic crystals that act in the visible wavelength range, e.g. structured polymer films [35], can be characterized. The technique also allows direct imaging of the topology of the FBZ of novel photonic structures, such as photonic quasi-crystals [29].

REFERENCES

1 Berthier, S. 2007 *Iridescences: the physical colors of insects.* New York, NY: Springer.

2 Kinoshita, S. 2008 *Structural colors in the realm of nature.* Singapore: World Scientific.

3 Srinivasarao, M. 1999 Nano-optics in the biological world: beetles, butterflies, birds, and moths. *Chem. Rev.* **99**, 1935–1962. (doi:10.1021/cr970080y)

4 Vukusic, P. & Sambles, J. R. 2003 Photonic structures in biology. *Nature* **424**, 852–855. (doi:10.1038/nature01941)

5 Stavenga, D. G., Wilts, B. D., Leertouwer, H. L. & Hariyama, T. 2011 Polarized iridescence of the multi-layered elytra of the Japanese jewel beetle, *Chrysochroa fulgidissima. Phil. Trans. R. Soc. B.* **366**, 709–723. (doi:10.1098/rstb.2010.0197)

6 Sharma, V., Crne, M., Park, J. O. & Srinivasarao, M. 2009 Structural origin of circularly polarized iridescence in jeweled beetles. *Science* **325**, 449–451. (doi:10.1126/science.1172051)

7 Galusha, J. W., Richey, L. R., Gardner, J. S., Cha, J. N. & Bartl, M. H. 2008 Discovery of a diamond-based photonic crystal structure in beetle scales. *Phys. Rev. E* **77**, 050904. (doi:10.1103/PhysRevE.77.050904)

8 Parker, A. R., Welch, V. L., Driver, D. & Martini, N. 2003 Structural colour: opal analogue discovered in a weevil. *Nature* **426**, 786–787. (doi:10.1038/426786a)

9 Joannopoulos, J. D. 2008 *Photonic crystals: molding the flow of light,* 2nd edn. Princeton, NJ: Princeton University Press.

10 Vukusic, P., Sambles, J. R., Lawrence, C. R. & Wootton, R. J. 1999 Quantified interference and diffraction in single *Morpho* butterfly scales. *Proc. R. Soc. Lond. B* **266**, 1403–1411. (doi:10.1098/rspb.1999.0794)

11 Leertouwer, H. L., Wilts, B. D. & Stavenga, D. G. 2011 Refractive index and dispersion of butterfly chitin and bird keratin measured by polarizing interference microscopy. *Opt. Express* **19**, 24 061–24 066. (doi:10.1364/OE.19.024061)

12 Wohlgemuth, M., Yufa, N., Hoffman, J. & Thomas, L. 2001 Triply periodic bicontinuous cubic microdomain morphologies by symmetries. *Macromolecules* **34**, 6083–6089. (doi:10.1021/ma0019499)

13 Michielsen, K. & Stavenga, D. G. 2008 Gyroid cuticular structures in butterfly wing scales: biological photonic crystals. *J. R. Soc. Interface* **5**, 85–94. (doi:10.1098/rsif.2007.1065)

14 Saranathan, V., Osuji, C. O., Mochrie, S. G., Noh, H., Narayanan, S., Sandy, A., Dufresne, E. R. & Prum, R. O. 2010 Structure, function, and self-assembly of single network gyroid ($I4_132$) photonic crystals in butterfly wing scales. *Proc. Natl Acad. Sci. USA* **107**, 11 676–11 681. (doi:10.1073/pnas.0909616107)

15 Hyde, S., Andersson, S., Larsson, K., Blum, Z., Landh, T., Lidin, S. & Ninham, B. 1997 *The language of shape: the role of curvature in condensed matter: physics, chemistry, and biology.* Amsterdam, The Netherlands: Elsevier.

16 Parker, A. R. & Townley, H. E. 2007 Biomimetics of photonic nanostructures. *Nat. Nanotechnol.* **2**, 347–353. (doi:10.1038/nnano.2007.152)

17 Sanchez, C., Arribart, H. & Guille, M. M. 2005 Biomimetism and bioinspiration as tools for the design of innovative materials and systems. *Nat. Mater.* **4**, 277–288. (doi:10.1038/nmat1339)

18 Juodkazis, S., Rosa, L., Bauerdick, S., Peto, L., El-Ganainy, R. & John, S. 2011 Sculpturing of photonic crystals by ion beam lithography: towards complete photonic bandgap at visible wavelengths. *Opt. Express* **19**, 5802–5810. (doi:10.1364/OE.19.005802)

19 Campbell, M., Sharp, D. N., Harrison, M. T., Denning, R. G. & Turberfield, A. J. 2000 Fabrication of photonic crystals for the visible spectrum by holographic lithography. *Nature* **404**, 53–56. (doi:10.1038/35003523)

20 Maldovan, M. & Thomas, E. L. 2004 Diamond-structured photonic crystals. *Nat. Mater.* **3**, 593–600. (doi:10.1038/nmat1201)

21 Pouya, C., Stavenga, D. G. & Vukusic, P. 2011 Discovery of ordered and quasi-ordered photonic crystal structures in the scales of the beetle *Eupholus magnificus. Opt. Express* **19**, 11 355–11 364. (doi:10.1364/OE.19.011355)

22 Stavenga, D. G., Leertouwer, H. L., Pirih, P. & Wehling, M. F. 2009 Imaging scatterometry of butterfly wing scales. *Opt. Express* **17**, 193–202. (doi:10.1364/OE.17.000193)

23 Johnson, S. & Joannopoulos, J. 2001 Block-iterative frequency-domain methods for Maxwell's equations in a planewave basis. *Opt. Express* **8**, 173–190. (doi:10.1364/OE.8.000173)

24 Michielsen, K. & Kole, J. 2003 Photonic band gaps in materials with triply periodic surfaces and related tubular structures. *Phys. Rev. B* **68**, 115107. (doi:10.1103/PhysRevB.68.115107)

25 Morrone, J. J. 2002 The neotropical weevil genus *Entimus* (Coleoptera: Curculionidae: Entiminae): Cladistics, biogeography, and modes of speciation. *Coleopt. Bull.* **56**, 501–513. (doi:10.1649/0010-065X(2002)056[0501:TNWGEC]2.0.CO;2)

26 Seago, A. E., Brady, P., Vigneron, J. P. & Schultz, T. D. 2009 Gold bugs and beyond: a review of iridescence and structural colour mechanisms in beetles (Coleoptera). *J. R. Soc. Interface* **6**(Suppl. 2), S165–S184. (doi:10.1098/rsif.2008.0354.focus)

27 Welch, V., Lousse, V., Deparis, O., Parker, A. & Vigneron, J. P. 2007 Orange reflection from a three-dimensional photonic crystal in the scales of the weevil *Pachyrrhynchus congestus pavonius* (Curculionidae). *Phys. Rev. E* **75**, 041919. (doi:10.1103/PhysRevE.75.041919)

28 Poladian, L., Wickham, S., Lee, K. & Large, M. C. 2009 Iridescence from photonic crystals and its suppression in butterfly scales. *J. R. Soc. Interface* **6**(Suppl. 2), S233–S242. (doi:10.1098/rsif.2008.0353.focus)

29 Man, W., Megens, M., Steinhardt, P. J. & Chaikin, P. M. 2005 Experimental measurement of the photonic properties of icosahedral quasicrystals. *Nature* **436**, 993–996. (doi:10.1038/nature03977)

30 Galusha, J. W., Jorgensen, M. R. & Bartl, M. H. 2010 Diamond-structured titania photonic-bandgap crystals from biological templates. *Adv. Mater.* **22**, 107–110. (doi:10.1002/adma.200902852)

31 Tan, Y., Gu, J., Zang, X., Xu, W., Shi, K., Xu, L. & Zhang, D. 2011 Versatile fabrication of intact three-dimensional metallic butterfly wing scales with hierarchical sub-micrometer structures. *Angew. Chem. Int. Ed. Engl.* **50**, 8307–8311. (doi:10.1002/anie.201103505;10.1002/anie.201103505)

32 Zang, X., Ge, Y., Gu, J., Zhu, S., Su, H., Feng, C., Zhang, W., Liu, Q. & Zhang, D. 2011 Tunable optical photonic devices made from moth wing scales: a way to enlarge natural functional structures' pool. *J. Mater. Chem.* **21**, 13 913–13 919. (doi:10.1039/c1jm12370j)

33 Chutinan, A., John, S. & Toader, O. 2003 Diffractionless flow of light in all-optical microchips. *Phys. Rev. Lett.* **90**, 123901. (doi:10.1103/PhysRevLett.90.123901)

34 Guldin, S., Huttner, S., Kolle, M., Welland, M. E., Muller-Buschbaum, P., Friend, R. H., Steiner, U. & Tetreault, N. 2010 Dye-sensitized solar cell based on a three-dimensional photonic crystal. *Nano Lett.* **10**, 2303–2309. (doi:10.1021/nl904017t)

35 Srinivasarao, M., Collings, D., Philips, A. & Patel, S. 2001 Three-dimensionally ordered array of air bubbles in a polymer film. *Science* **292**, 79–83. (doi:10.1126/science.1057887)